Tribological properties of picosecond laser-textured titanium alloys under different lubrication conditions

[1] Jialiang Guo, [1, 2, 3, 4] Fang Wang, [1, 2, 3] Juin J. Liou and [1, 2, 3, 4] Yuhuai Liu

[1] National Center for International Joint Research of Electronic Materials and Systems, International Joint-Laboratory of Electronic Materials and Systems of Henan Province, School of Electrical and Information Engineering, Zhengzhou University, 100 Science Avenue, Fengyang Street, High-Tech District, Zhengzhou, Henan 450001, China, ieyhliu@zzu.edu.cn
[2] Institute of Intelligence Sensing, Zhengzhou University, 100 Science Avenue, Fengyang Street, High-Tech District, Zhengzhou, Henan 450001, China, iefwang@zzu.edu.cn
[3] Research Institute of Industrial Technology Co. Ltd., Zhengzhou University, 11 Changchun Road, Wutong Street, High-tech District, Zhengzhou, Henan 450001, China
[4] Zhengzhou Way Do Electronics Co. Ltd., 11 Changchun Road, Wutong Street, High-tech District, Zhengzhou, Henan 450001, China

Received: 29.09.2022

Abstract. Laser surface texturing has repeatedly demonstrated great potentials for improving a wear resistance. It represents a simple, highly efficient and controllable tool. To increase the utility of Ti-6Al-4V titanium alloy in complex industrial-application environments, we suggest a highly reproducible hydrophobic wear-resistant surface-preparation method. The surface morphology, the chemical composition and the wettability of a fluorinated picosecond laser-textured titanium alloy are analyzed experimentally. A ball-disk reciprocating friction test is used to examine the tribological properties of a Si_3N_4 ball sliding against a titanium-alloy surface under different lubrication conditions. The effects of laser-texturing pattern and scanning interval on the water-contact angle and the coefficient of friction (CoF) are studied. In general, the surfaces with sparse scanning intervals exhibit low CoFs under dry and water-lubricated conditions. Under dry, water- and oil-lubricated conditions, the CoF of the textured surfaces decreases respectively by up to 18, 21 and 60%, if compared with that of the original surface.

Keywords: picosecond lasers, surface textures, titanium alloys, wettability, friction coefficient

UDC: 621.7+535

1. Introduction

Wear between friction pairs is a primary factor in the reduction of working efficiency, safety and lifespan of components in mechanical drives [1]. In the field of mineral exploitation alone, annual losses caused by friction and wear can exceed €200 billion [2]. In the natural world, organisms have evolved surfaces with the structures adapted to their surrounding environment, as in lotus leaves [3], shark skin [4] or butterfly wings [5]. Inspired by these natural surface structures, hydrophobic surfaces regulated by micro/nanostructures and low-energy surfaces have been successfully developed. They are widely used in various applications such as metal-corrosion prevention [6], fluid-drag reduction [7], ice and fog prevention [8] and oil–water separation [9]. Recently, the role of the surfaces with microstructures has been increasingly recognized for the improvement of surface-frictional properties [10].

Currently, such techniques as electrochemical machining [11], electrical-discharge machining [12], abrasive-jet machining [13], photolithographic etching [14], reactive-ion etching [15] and anisotropic etching [16] are used to produce microstructural surfaces. Moreover, laser surface texturing based upon ultrashort-pulse lasers is a new promising method for preparing microstructures. It improves tribological performance of materials and represents a highly efficient, controllable and environmentally friendly technique which can be applied to metallic materials [17, 18].

Kumar et al. [19] have investigated the effect of laser-texturing density and shape on the tribological characteristics of 100Cr6-bearing steel surfaces under dry-friction conditions. They have shown that a compact bi-triangular texture reveals a lower coefficient of friction (CoF), along with strengthened fatigue resistance of a 100Cr6 surface. This implies expanded applications of the latter in high-precision ball and roller bearings. Huang et al. [20] have prepared pit-textured pure-nickel surfaces using a nanosecond laser and shown that the CoF of the textured surface decreases by more than 70% when compared with that of the original surface under water-lubricated conditions. Jendoubi et al. [21] have used a femtosecond laser to ablate polytetrafluoroethylene and prepared superhydrophobic surfaces with micron-scale hexagonal small-pore-array structures. Their textured surfaces show a higher CoF under water-lubricated conditions in comparison with the polished surfaces. This could be explained by a high-pressure-induced wettability transition and vortexing. In spite of significant advance, the works mentioned above have dealt only with the analysis of a single lubricating condition. Still, there is a lack of the studies addressing the tribological behaviour of the laser-textured surfaces under different lubrication conditions.

In the present work, we have selected a Ti-6Al-4V alloy as a substrate material. It represents the most commonly used biphasic titanium alpha-beta alloy. The appropriate composition involves 6% of aluminium, 4% of vanadium, 0.25% of iron, 0.2% of oxygen and the rest of titanium. Different textured surfaces with periodic micron-scale groove arrays have been prepared on the Ti-6Al-4V alloy surfaces by sequentially using a picosecond laser ablation and a self-assembly chemical modification. Surface characterization, surface chemical-composition analysis, water contact-angle (WCA) measurements and CoF-oriented friction tests have been used to investigate the wettability and the tribological properties of the specimens prepared in this manner. The effects of different texture patterns (including parallel, crossed and wavy grooves) and different groove spacings have been investigated. The methodology and the findings of this study can be used as a theoretical reference for practical applications of different textures built on the titanium-alloy components.

2. Materials and methods

Ti-6Al-4V alloy rods with the diameter of 25 mm (Shenyulanjing Metal Materials Co., Ltd., Baoji, China) were used as a substrate material. They were cut into 7-mm-thick discs and mechanically polished to a surface roughness (Sa) of approximately 0.2 μm. Before and after laser treatment, the specimens were cleaned in an ultrasonic bath for 10 min with analytical-grade petroleum ether (Shanghai Macklin Biochemical Co., Ltd., Shanghai, China) and absolute ethanol (Guangdong Guanghua Sci-Tech Co., Ltd., Shantou, China).

Vanadate crystals are among the main materials used in medium- and low-power all-solid-state lasers. They manifest large absorption and emission cross-sections. In this study, a neodymium-doped yttrium orthovanadate ($Nd:YVO_4$) picosecond laser (PX100-3-GF, Edgewave, Germany) with the central wavelength 355 nm was employed to ablate our specimens and texture the titanium-alloy surfaces. The laser beam propagated through an f–θ lens with the focal length of 100 mm and was focused on the specimen surface. The spot diameter was equal to 15 μm. The laser-processing parameters were as follows: the repetition frequency 800 kHz, the scanning speed 200 mm/s, the pulse width 10 ps, and the output power 7 W. The previous study [22] had confirmed that the groove depth increased with increasing number of laser-processing cycles and that deep grooves were one of the main factors ensuring beneficial tribological properties of the textured surfaces. As the laser power used in this study was low, the specimens were processed during 40 cycles to ensure a sufficient groove depth.

As shown in Fig. 1, the specimens were textured with periodic microgrooves. The grooves were approximately 12 μm wide, and the groove spacings 35, 40, 50, 60, 70 and 100 μm were produced by adjusting the path and the intervals of laser scanning. Three groove patterns were used: parallel grooves, crossed grooves with the crossing angle 90°, and wavy grooves with the wave angle 90° and the amplitude 113 μm.

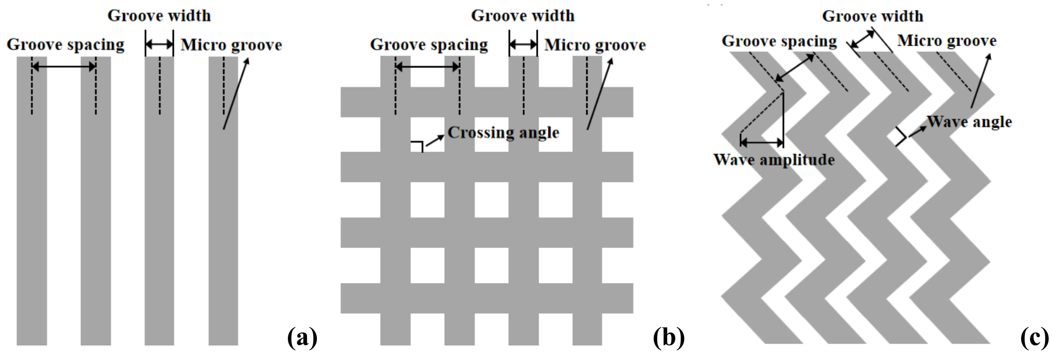

Fig. 1. Scheme of surface textures formed in this work. The groove patterns include (a) parallel, (b) crossed and (c) wavy grooves.

As mentioned above, Jendoubi et al. [21] had noted that the surfaces textured via laser alone were prone to larger CoFs, if compared with the corresponding parameters typical for the original surfaces under water-sliding conditions. Therefore, we applied a self-assembly-based fluorination treatment to the textured surfaces. A 97 wt. % fluoroalkyl silane $C_8H_4Cl_3F_{13}Si$ (1H,1H,2H,2H-perfluorooctyl trichlorosilane, FOTS) solution (Meryer Chemical Technology Co., Ltd., Shanghai, China) was diluted to 3 wt. %, using analytical-grade isooctane (Meryer Chemical Technology Co., Ltd., Shanghai, China). The specimens were irradiated with ultraviolet light continuously for 1 h and then treated chemically by immersing them into the FOTS solution for 2 h. The ultraviolet irradiation ensured that there were abundant hydroxyl groups on the surface of the titanium alloy, which facilitated attachment of FOTS molecules. After chemical treatment, the specimens were subjected to successive ultrasonic baths in petroleum ether, absolute ethanol and deionized water (produced in our laboratory) for 10 min. Finally, they were completely dried in an oven.

A confocal-laser scanning microscope (LEXT™ OLS5100, Olympus, Japan) was used to plot three-dimensional profiles of the specimen surfaces. A scanning electron microscope (SEM) Prisma E from Thermo Fisher Scientific (USA) was used to observe the morphology of the specimens, whereas an energy-dispersive X-ray spectroscopy was employed to determine their surface chemical compositions. For the wettability analysis, 3 μL of deionized water was dropped onto the surface of each specimen. The droplet profiles were automatically captured by an optical contact-angle measuring and contact-analysis system (OCA25, DataPhysics, Germany). The

WCAs of our specimens were calculated using the Laplace–Young equation [23]. For each specimen, the WCA was measured at five different positions to ensure statistical significance.

As shown in Fig. 2, tribological tests were conducted using a ball-on-disc universal tribometer (UMT-5, Bruker, USA) with linear reciprocating sliding, and time dependences of the CoF were recorded continuously. For each surface, a 10-mm-diameter Si_3N_4 antithesis ball slid continuously for 600 s at the speed of 12 mm/s under a normal load of 5 N. The average CoF during sliding was calculated. Deionized water and fully synthetic automatic transmission oil (EasyCheer, ATF6, China) with the kinematic viscosity 27.47 at 25°C and the viscosity index 157 were selected as sliding lubricants. The tribological tests were repeated three times for each specimen under different lubrication conditions (i.e., dry, water and oil lubrication).

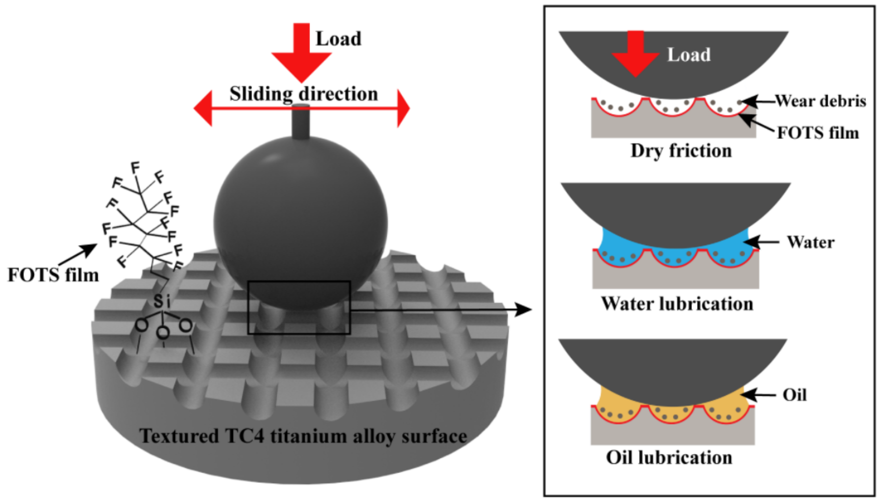

Fig. 2. Scheme of a system used for testing tribological properties.

3. Results and discussion

3.1. Surface morphology

Fig. 3 shows the three-dimensional profiles and the profile lines obtained for the surfaces with the parallel, crossed and wavy grooves (at the groove spacing 40 μm). The microgrooves are regularly arranged on the titanium-alloy surface. The depth and the width of each groove are approximately equal to 12.1 and 10.7 μm, respectively. Slight microbulges are present on both sides of the grooves and there is a little effect in the areas which have not been scanned by the laser.

Fig. 4 displays the SEM images and the energy-dispersive X-ray spectroscopy data obtained after laser and chemical treatments for the specimens with different groove patterns. These results refer to the groove spacing 40 μm. The heat-affected area surrounding the microgrooves is very narrow and a few re-melted or regenerated particles can be found on the surface of our titanium alloy owing to direct gasification of the picosecond-laser-irradiated area. A nanoscale corrugated structure inside the microgrooves, which is caused by repeated laser processes, can be seen in the magnified SEM images. When the chemical treatment has not been performed, the oxygen content of the textured area is significantly higher than that of the non-textured area. This indicates that strong oxidation occurs after the specimen is processed by the picosecond laser. After the chemical treatment, Si and F can be detected as new surface elements, while the content of C becomes enhanced. These facts testify that a molecular FOTS film is successfully self-assembled on the surface of our specimen.

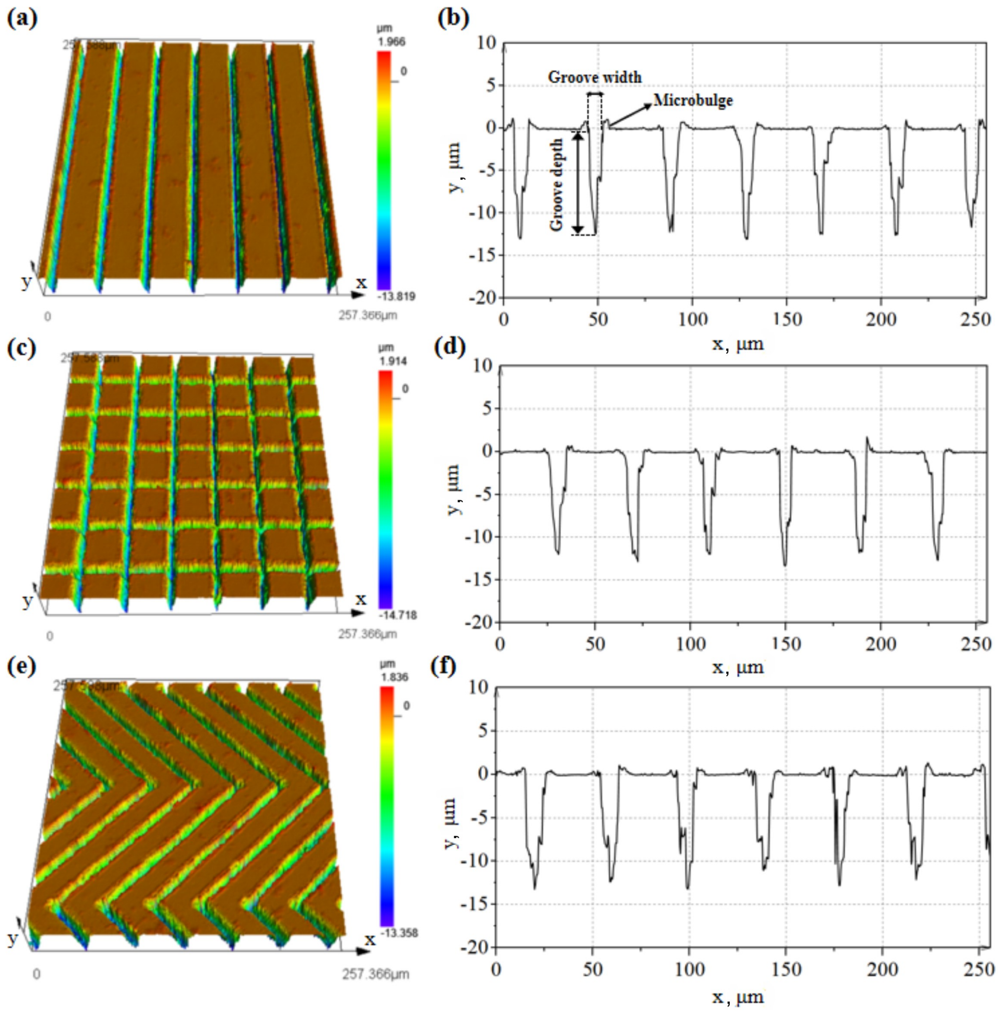

Fig. 3. Three-dimensional profiles (left) and profile lines (right) obtained for titanium-alloy surfaces with different groove patterns (the groove spacing 40 µm): panels (a) and (b), (c) and (d), and (e) and (f) correspond respectively to parallel, crossed, and wavy grooves.

3.2. Wettability

Fig. 5 shows the WCA images obtained for the polished titanium-alloy surfaces at different treatment stages. The WCA of the polished and laser-ablated surfaces are equal respectively to 68.2±3.3° and 32.4±5.1°. The hydrophilicity is enhanced due to abundance of Ti_xO_y on the laser-ablated surface of the titanium alloy. Oxygen cavities on the surface are easily replaced by water molecules in the air to form hydroxyl groups. The ultraviolet irradiation intensifies this process and increases greatly the free energy of the surface. When the specimens are immersed in the FOTS solution, the FOTS molecules undergo a dehydration condensation reaction with the hydroxyl groups on the titanium-alloy surface where they are self-assembled, thus producing a hydrophobic effect. After the fluorination treatment, the WCA of the polished surface becomes 110±2.4°, whereas the same parameter for the surface with the crossed grooves and the groove spacing 35 µm is equal to 143.8±1°, which is close to the superhydrophobic state (WCA > 150°).

Fig. 6. shows the dependences of WCA on the groove spacing, which have been obtained for different grooved patterns. For each texture pattern and fixed laser parameters, the WCA decreases

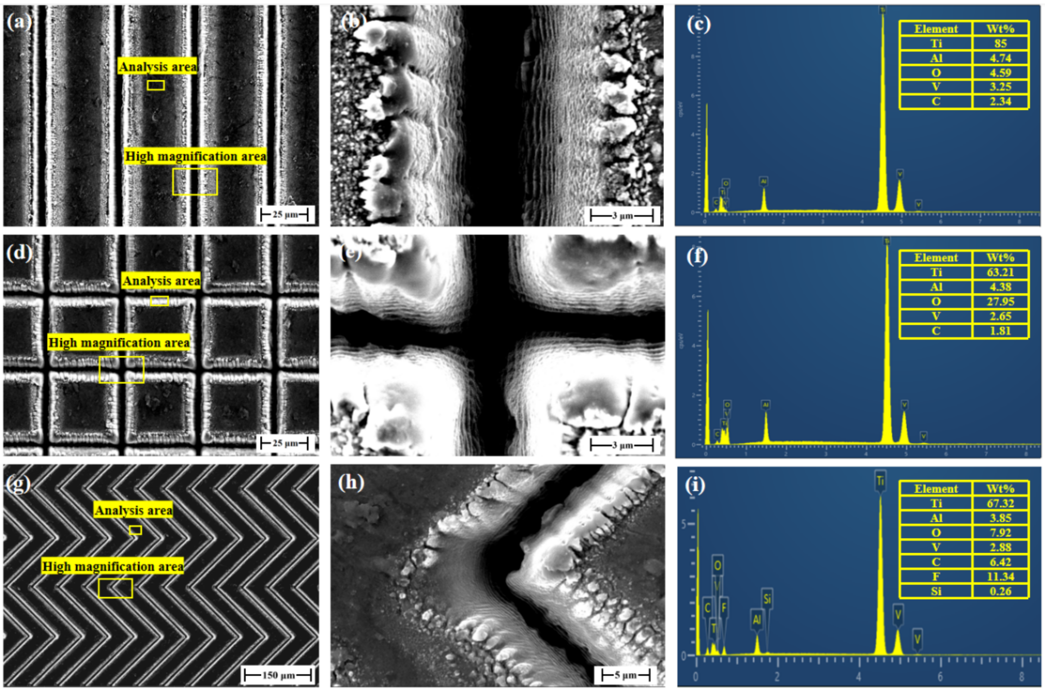

Fig. 4. SEM images and energy-dispersive X-ray spectroscopy data obtained for our titanium-alloy surfaces with different groove patterns: panels (a)–(c), (d)–(f) and (g)–(i) refer respectively to the parallel grooves (laser treatment only), crossed grooves (laser treatment only) and wavy grooves (two-step laser-and-chemical treatment). Left, middle and right rows of figures correspond respectively to normal SEM images, high-magnification SEM images and energy-dispersive X-ray spectroscopy data. The groove spacing amounts to 40 μm in all cases.

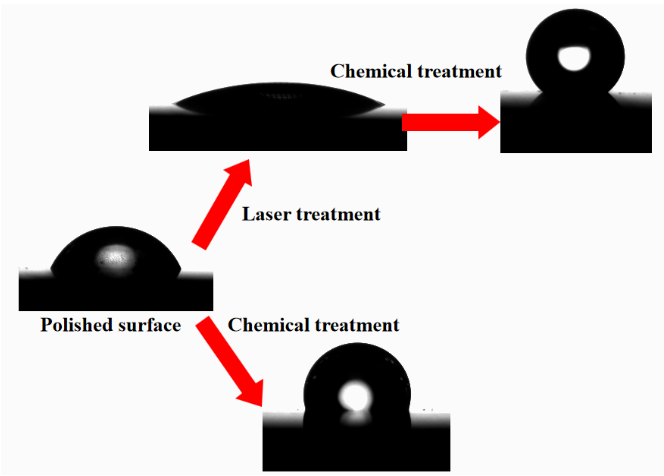

Fig. 5. WCA patterns (i.e., side views of water droplets situated on the polished titanium-alloy surface) observed at different treatment steps.

with increasing groove spacing. A minimal WCA, 127±1.9°, is observed for the surface with the parallel grooves and the groove spacing 100 μm. For a given groove spacing, the maximal WCA is always observed for the surface with the crossed grooves. The groove spacing has the least effect for the surface with the wavy grooves: the WCA for this groove pattern decreases by only ~ 5° (from 131.7±2.7° to 136.8±2.4°) as the groove spacing increases from 35 to 100 μm. According to Cassie and Baxter [24], the change in the WCA depends on the microstructural difference resulting from different laser-scanning intervals. This can be expressed as follows: $\cos\theta_{CB} = F_S(\cos\theta_S + 1)^{-1}$, where θ_{CB} and θ_s are the WCAs of the textured and ideal smoothly polished surfaces, respectively, and F_s is the fraction of the contact area occupied by the solid interface. Denser grooves provide a smaller F_s, hence the θ_{CB} parameter becomes larger.

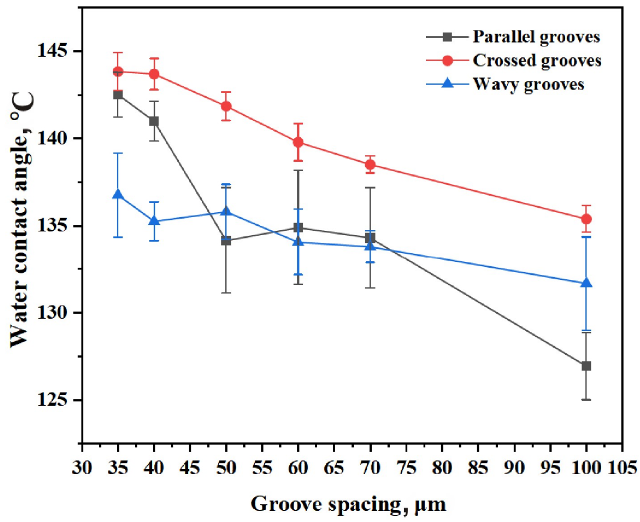

Fig. 6. Dependences of WCA on the groove spacing for the fluorinated titanium-alloy surfaces with different groove patterns (see the legend).

3.3. Tribological properties

Fig. 7. shows the average CoF for different surfaces under dry, water-lubricated and oil-lubricated sliding conditions. Under the dry conditions, the average CoF of the polished surface is approximately equal to 0.427. As the groove spacing increases from 35 to 100 μm, the average CoF of the surfaces with the parallel and wavy grooves decreases in general. Under these conditions, the maximal average CoF 0.448 is observed for the surface with the wavy grooves and the groove spacing 40 μm. This can be attributed to the fact that the actual contact area is small due to a compact groove arrangement, which transforms elastic deformation into plastic one [25]. The wavy microgrooves intensify this effect and increase the friction force.

The average CoFs for the surfaces with the crossed grooves are approximately 0.42. Here the groove spacing has a little effect on the CoF. This is probably because the Si_3N_4 ball is much larger than the grooves, so that it remains always in contact with many microgrooves during sliding and, moreover, it collides with the microbulges on the sides of the grooves. This results in more or less consistent friction [26]. Under this condition, the minimal average CoF 0.349 is observed for the surface with the parallel grooves and the groove spacing 100 μm. A larger groove spacing may have reduced the friction caused by the microbulges. Thus, the effect of microgrooves capturing wear debris is significant: it reduces the adhesion wear [27].

Under the water-lubricated sliding conditions, the average CoF of the polished surface amounts to 0.41. It is slightly lower than that observed under the dry conditions because the water washes away the debris. As for the dry sliding conditions, the average CoF decreases with increasing groove spacing, which indicates that the mechanisms of CoF behaviour under the dry and water-lubricated conditions are similar. The average CoFs measured for all the grooved surfaces are less than 0.4, with the mean value being around 0.35. There are several reasons for these experimental observations. First, a hydrophobic surface has a lower surface energy, which reduces the adhesion of the contacted surface [28]. Second, the shear strength between the sliding solid surfaces is reduced by water [29]. And third, the grooves promote hydrodynamic lubrication under the water-lubricated sliding conditions, which increases the load-carrying capacity of our titanium-alloy surface [30]. Under this condition, one can observe the minimal average CoF 0.325 for the surface with the wavy grooves and the groove spacing 70 μm.

Under the oil-lubricated sliding conditions, the average CoF measured for the polished surface is approximately 0.28. This demonstrates that the oil has a better anti-wear effect than the air and the water whenever it is spread on the surface of the material as a lubricant. The average CoFs detected for the grooved surfaces remain below 0.15, which is 50% lower than that of the polished surface under the same conditions. This may be caused by superposition of the oil-storage and debris-capturing effects of the microgrooves. In other words, the microgrooves provide a sliding interface with a steady supply of stored oil and also collect and store the debris [31]. Moreover, the hydrodynamic lubrication enhances the load-carrying capacity of the lubricating oil film, which further reduces the average CoF. Under this condition, the minimal average CoF 0.112 is observed for the surface with the wavy grooves and the groove spacing 35 μm. As the groove spacing increases, the microgrooves do not provide sufficient oil to the sliding surface and the debris is not captured efficiently, which increases the average CoF.

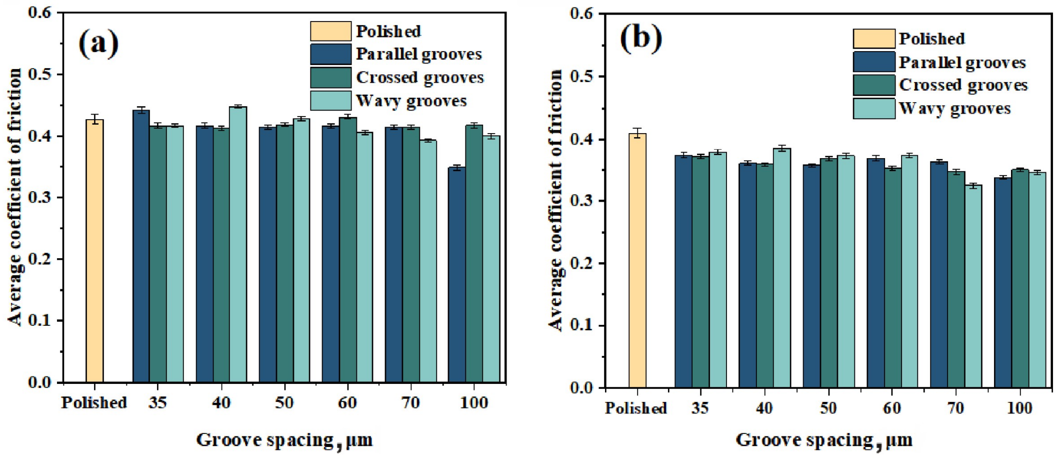

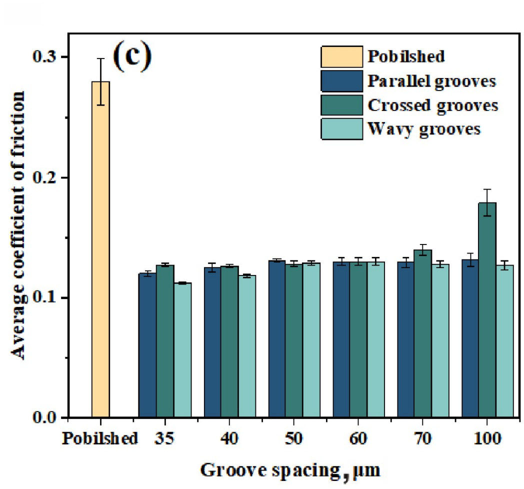

Fig. 7. Average CoF of our titanium-alloy surfaces with different groove patterns (see the legend) as a function of groove spacing. The measurements correspond to (a) dry, (b) water-lubricated and (c) oil-lubricated sliding conditions.

Fig. 8. shows the time dependences of the CoF, which are measured for three representative surfaces under different lubrication conditions. For the polished surfaces, the CoF exceeds 0.45 when sliding begins due to poor wear resistance. A similar trend can be seen under the water-lubricated conditions, where a slight increase over time occurs. Under the oil-lubricated conditions, the CoF decreases from approximately 0.4 to 0.25 and then fluctuates between 0.25 and 0.35. This indicates that a stable oil film is not formed on the polished surface during sliding; accordingly, the system switches between friction-pair contact and dry friction [32].

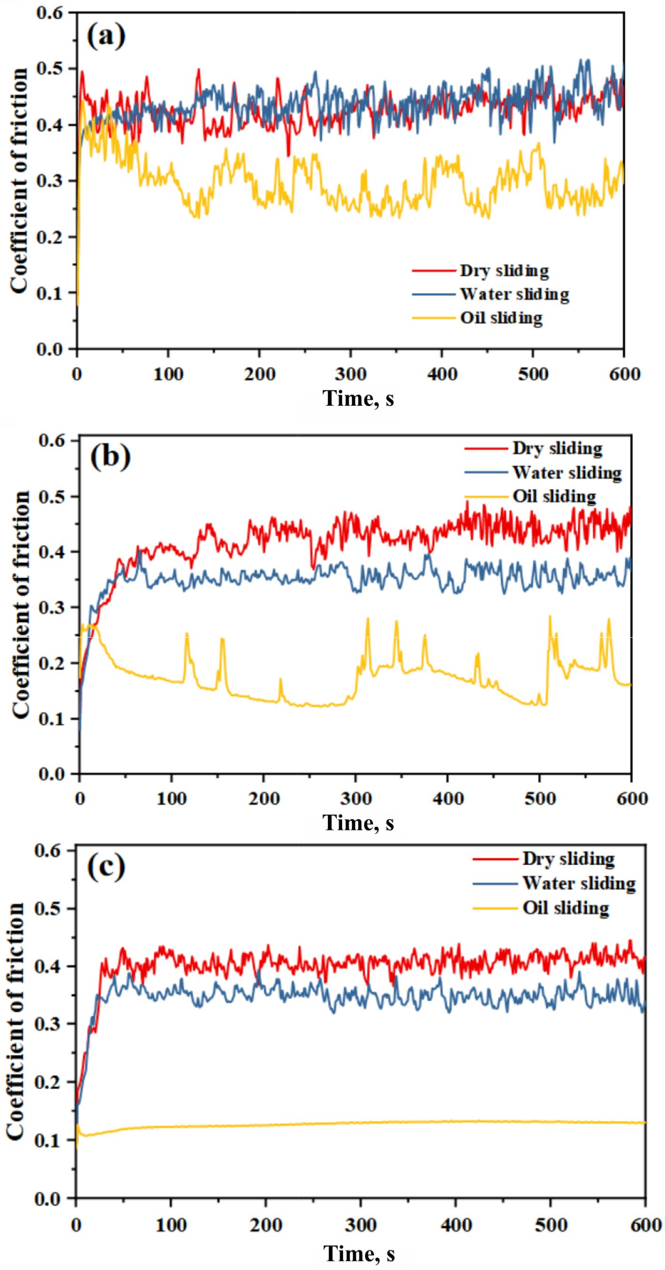

Fig. 8. Time variations of CoF for three representative surfaces, as measured under dry, water-lubricated and oil-lubricated sliding conditions (see the legend): (a) polished surface, (b) fluorinated surface with crossed grooves and the groove spacing 100 μm, and (c) fluorinated surface with wavy grooves and the groove spacing 100 μm.

When the groove spacing is equal to 100 μm, the surfaces with the crossed and wavy grooves manifest similar CoF trends under the dry and water-lubricated conditions. Initially, their CoFs increase at approximately the same rate. Then the CoF of the water-lubricated surfaces fluctuates about 0.35, whereas the CoF of the dry surfaces fluctuates about 0.4. Under the oil-lubricated conditions, the CoF of the surface with the crossed grooves fluctuates greatly and there are many changes in the shapes of spikes seen on the curve. This demonstrates that the oil film is easily destroyed and the dry friction is constantly competing with the oil film during sliding. In contrast, the CoF of the surface with the wavy grooves increases slowly from 0.11 to 0.13 between 5 and 300 s. Then it remains stable, thus indicating that a continuous oil film has formed on the titanium-alloy surface.

4. Conclusions

In this study, the picosecond laser has been used to ablate the surfaces of the Ti-6Al-4V alloy specimens in order to produce different surface textures consisting of parallel, crossed and wavy grooves. The morphologies and the chemical compositions of the surfaces have been analyzed, and their wettability and tribological properties have been investigated after the fluorination treatment. The main conclusions of our study can be summarized as follows.

(1) Due to a thermal effect, there are Ti_xO_y-rich microbulges on both edges of the microgrooves ablated by the picosecond laser. The interior of the microgrooves has a corrugated structure. The C content in the titanium-alloy surface increases after the fluorination treatment. Moreover, F and Si also begin to appear under this condition.

(2) A combination of the laser and chemical treatments changes the wettability of the titanium-alloy surface from highly hydrophilic to nearly superhydrophobic. The WCA decreases with increasing groove spacing on the textured surfaces (from 35 to 100 μm). The surface with the crossed grooves has a higher WCA, and the wettability of the surface with the wavy grooves is modestly affected by the groove spacing.

(3) The fluorinated textured surfaces retain some anti-wear properties, while their tribological properties can be governed by adjusting the groove pattern and the groove spacing. The CoFs of the polished surface are equal to 0.427, 0.41 and 0.28 respectively under the dry, water-lubricated and oil-lubricated sliding conditions. The corresponding minimal CoFs of the textured surfaces amount to 0.349, 0.325 and 0.112, which corresponds to 18, 21 and 60% reductions.

The method offered in the present work improves greatly the surface properties of the titanium alloys. It can also be expected to reduce the impact of fretting wear on the service life of the structural parts made of titanium alloys in many complex industrial environments such as oil wells and underwater operations. Note also that our findings and conclusions are almost entirely based on experimental observations. Therefore, theoretical foundations and numerical simulations of the wear-reduction effect found experimentally in the present work for the hydrophobic textured surfaces should be explored in the future.

Acknowledgements. This work was supported by the National Nature Science Foundation of China (the Project #62174148), the National Key Research and Development Program (##2022YFE0112000 and 2016YFE0118400), the Zhengzhou 1125 Innovation Project (#ZZ2018-45), and the Ningbo 2025 Key Innovation Project (#2019B10129). These grants were issued to Professor Yuhuai Liu.

Conflicts of interest. The authors declare that they do not have any commercial or associative interests that represent a conflict of interest in connection with this work.

Data availability. The data that support the findings of this study are available from the corresponding authors upon reasonable request.

References

1. Marian M, Berman D, Rota A, Jackson R L and Rosenkranz A, 2022. Layered 2D nanomaterials to tailor friction and wear in machine elements – a review. Adv. Mater. Interfaces. **9**: 2101622.
2. Holmberg K, Kivikytö-Reponen P, Härkisaari P, Valtonen K and Erdemir A, 2017. Global energy consumption due to friction and wear in the mining industry. Tribol. Int. **115**: 116–139.
3. Ghasemlou M, Le P H, Daver F, Murdoch B G, Ivanova E P and Adhikari B, 2021. Robust and eco-friendly superhydrophobic starch nanohybrid materials with engineered lotus leaf mimetic multiscale hierarchical structures. ACS Appl. Mater. Interfaces. **13**: 36558–36573.
4. Liu Y, Gu H, Jia Y, Liu J, Zhang H, Wang R, Zhang B, Zhang H and Zhang Q, 2019. Design and preparation of biomimetic polydimethylsiloxane (PDMS) films with superhydrophobic, self-healing and drag reduction properties via replication of shark skin and SI-ATRP. Chem. Eng. J. **356**: 318–328.
5. Shao C, Chi J, Chen Z, Cai L and Zhao Y, 2019. Superwettable colloidal crystal micropatterns on butterfly wing surface for ultrasensitive detection. J. Colloid Interface Sci. **546**: 122–129.
6. Boinovich L B, Emelyanenko A M, Modestov A D, Domantovsky A G and Emelyanenko K A, 2015. Synergistic effect of superhydrophobicity and oxidized layers on corrosion resistance of aluminum alloy surface textured by nanosecond laser treatment. ACS Appl. Mater. Interfaces. **7**: 19500–19508.
7. Xin G, Wu C, Cao H, Liu W, Li B, Huang Y, Rong Y and Zhang G, 2020. Superhydrophobic TC4 alloy surface fabricated by laser micro-scanning to reduce adhesion and drag resistance. Surface and Coatings Technol. **391**: 125707.
8. Volpe A, Gaudiuso C and Ancona A, 2020. Laser fabrication of anti-icing surfaces: a review. Mater. **13**: 5692.
9. Ahlawat S, Singh A, Mukhopadhyay P K, Singh R and Bindra K S, 2021. Nanosecond laser induced glass particle deposition over steel mesh for long-term superhydrophilicity and gravity driven oil water separation. Mater. Chem. Phys. **263**: 124343.
10. Schille J, Schneider L, Mauersberger S, Szokup S, Höhn S, Pötschke J, Reiß F, Leidich E and Löschner U, 2020. High-rate laser surface texturing for advanced tribological functionality. Lubricants. **8**: 33.
11. Qian S, Ji F, Qu N and Li H, 2014. Improving the localization of surface texture by electrochemical machining with auxiliary anode. Mater. Manuf. Processes. **29**: 1488–1493.
12. Karmiris-Obratański P, ZagórskiK, Papazoglou E L and Markopoulos A P, 2021. Surface texture and integrity of electrical discharged machined titanium alloy. Int. J. Adv. Manuf. Technol. **115**: 733–747.
13. 13 Su X, Shi L, Huang W and Wang X, 2016. A multi-phase micro-abrasive jet machining technique for the surface texturing of mechanical seals. Int. J. Adv. Manuf. Technol. **86**: 2047–2054.
14. Xu Y, Yu J, Geng J, Abuflaha R, Olson D, Hu X and Tysoe W T, 2018. Characterization of the tribological behavior of the textured steel surfaces fabricated by photolithographic etching. Tribol. Lett. **66**: 1–15.
15. Ahn S, Park H, Cho J, Park C, Park J, Lee H, Hong K and Bong S, Yi J, 2021. Reactive-ion-etched glass surface with 2D periodic surface texture for application in solar cells. Optik. **229**: 166304.

16. King D L and Buck M E, Experimental optimization of an anisotropic etching process for random texturization of silicon solar cells. Sandia National Laboratories, Albuquerque, New Mexico, 1991.
17. Bonse J, Kirner S V, Griepentrog M, Spaltmann D and Krüger J, 2018. Femtosecond laser texturing of surfaces for tribological applications. Mater. **11**: 801.
18. Bertolete M, Barbosa P A, Machado ÁR, Samad R E, Vieira N D, Vilar R and De Rossi W, 2018. Effects of texturing the rake surfaces of cemented tungsten carbide tools by ultrashort laser pulses in machining of martensitic stainless steel. Int. J. Adv. Manuf. Technol. **98**: 2653–2664.
19. Kumar M, Ranjan V and Tyagi R, 2020. Effect of shape, density, and an array of dimples on the friction and wear performance of laser textured bearing steel under dry sliding. J. Mater. Eng. Perform. **29**: 2827–2838.
20. Huang J, Zhang L, Wei S, Yang Y, Yang S and Shen Z, 2019. Fabrication of the laser textured nickel surface and its tribological property under the water lubrication. AIP Adv. **9**: 085224.
21. Jendoubi H, Smerdova O and Brunetière N, 2021. Unexpected frictional behavior of laser-textured hydrophobic surfaces. Lubricants. **9**: 31.
22. Huang J, Wei S, Zhang L, Yang Y, Yang S and Shen Z, 2019. Fabricating the superhydrophobic nickel and improving its antifriction performance by the laser surface texturing. Mater. **12**: 1155.
23. Young T, 1805. An essay on the cohesion of fluids. Philos. Trans. Roy. Soc. London. **95**: 65–87.
24. Cassie A B D and Baxter S, 1944. Wettability of porous surfaces. Faraday Society. **40**: 546–551.
25. Wang Z, Zhao Q, Wang C and Zhang Y, 2015. Modulation of dry tribological property of stainless steel by femtosecond laser surface texturing. Appl. Phys. A. **119**: 1155–1163.
26. Ding Q, Wang L, Hu L, Hu T and Wang Y, 2012. The pairing-dependent effects of laser surface texturing on micro tribological behavior of amorphous carbon film. Wear. **274–275**: 43–49.
27. Xing Y, Deng J, Feng X and Yu S, 2013. Effect of laser surface texturing on Si_3N_4/TiC ceramic sliding against steel under dry friction. Mater. Des. (1980–2015). **52**: 234–245.
28. Kalin M and Polajnar M, 2013. The effect of wetting and surface energy on the friction and slip in oil-lubricated contacts. Tribol. Lett. **52**: 185–194.
29. Meng H, Sui G X, Xie G Y and Yang R, 2009. Friction and wear behavior of carbon nanotubes reinforced polyamide 6 composites under dry sliding and water lubricated condition. Compos. Sci. Technol. **69**: 606–611.
30. Wang W, He Y, Zhao J, Mao J, Hu Y and Luo J, 2020. Optimization of groove texture profile to improve hydrodynamic lubrication performance: theory and experiments. Friction. **8**: 83–94.
31. Shum P W, Zhou Z F and Li K Y, 2013. Investigation of the tribological properties of the different textured DLC coatings under reciprocating lubricated conditions. Tribol. Int. **65**: 259–264.
32. Flegler F, Neuhäuser S and Groche P, 2020. Influence of sheet metal texture on the adhesive wear and friction behaviour of EN AW-5083 aluminum under dry and starved lubrication. Tribol. Int. **141**: 105956.

Jialiang Guo, Fang Wang, Juin J. Liou and Yuhuai Liu. 2022. Tribological properties of picosecond laser-textured titanium alloys under different lubrication conditions. Ukr.J.Phys.Opt. **23**: 243 – 255. doi: 10.3116/16091833/23/4/243/2022

***Анотація**. Лазерне текстурування поверхні виявляє значний потенціал для підвищення зносостійкості та є простим, високоефективним і керованим інструментом. Щоб підвищити корисність титанового сплаву Ti-6Al-4V у складних промислових середовищах,* *ми пропонуємо високовідтворюваний гідрофобний зносостійкий метод підготовки поверхні. Досліджено та проаналізовано морфологію поверхні, хімічний склад і змочуваність фторованого, текстурованого пікосекундним лазером титанового сплаву. Для вивчення трибологічних властивостей кульки Si_3N_4, що ковзає по поверхні титанового сплаву за різних умов змащування, вжито тест зворотно-поступального тертя кулька–диск. Досліджено вплив візерунка лазерного текстурування та інтервалу сканування на кут контакту з водою та на коефіцієнт тертя (КТ). Загалом, поверхні з рідкими інтервалами сканування демонструють низькі значення КТ у сухих і змащених водою умовах. У сухих умовах, а також умовах змащування водою та оливою, КТ текстурованих поверхонь зменшується відповідно на 18, 21 і 60%, порівняно з показником для вихідної поверхні.*

Ключові слова: *пікосекундні лазери, текстура поверхні, титанові сплави, змочуваність, коефіцієнт тертя*